INVESTIGATION OF THE INFLUENCE OF THE REYNOLDS NUMBER ON THE PREDICTION ACCURACY OF LAMINAR DRAG COMPONENTS

T. Effing, F. Schueltke, E. Stumpf
Institute of Aerospace Systems, RWTH Aachen University
Wuellnerstraße 7, 52062 Aachen, Germany

Abstract

The preliminary aerodynamic design of aircraft with integrated hybrid laminar flow technology essentially consists of a reliable and robust transition prediction and the estimation of laminar drag polars under given wing geometry and flow conditions. Using an in-house developed process chain for laminar flow analysis, the effects of the Reynolds number on various instability mechanisms and the corresponding transition location are derived within this study. With constant design parameters (Mach number, lift coefficient, and suction distribution), the destabilization of the boundary layer can be fundamentally attributed to the Reynolds number as a decisive factor. Similar to the theory of a flat plate, a critical Reynolds number is defined, exceeding which leads to an abrupt shift of the transition location. In addition, the influence of varying wing geometry parameters on this critical threshold is investigated. Based on the presented findings, a necessity for extending the existing process chain is derived in order to adequately reflect the influence of the Reynolds number. The advantages of the adapted method are shown in a comparative application example using an Airbus A350-900 preliminary design. By taking the influence of the Reynolds number into account, a considerable increase in prediction accuracy of laminar drag components is achieved. Furthermore, it is briefly discussed that varying the suction distribution can lead to a complete avoidance of above mentioned transition shifts and thus to a significant reduction of laminar drag components.

Keywords Reynolds number, Instability mechanisms, Hybrid laminar flow control, Conceptual aircraft design

1. Introduction

The global aviation industry is not only affected by a constantly growing passenger volume, but also by the desire for greater economic efficiency while simultaneously minimizing emissions. Further progress with regard to fuel efficiency of future aircraft is possible by optimizing the aerodynamic layout. One promising technique is the hybrid laminar flow control (HLFC), as it can reduce viscous drag. Since this drag component adds up to more than 50 % of the overall aircraft drag in cruise [1], HLFC has the potential to significantly reduce fuel consumption [2], [3]. As the HLFC technology is still in research stage, the informative value of the actual efficiency gain must be as high as possible already for conceptual aircraft design. Therefore, understanding the influence of a fundamental key variable such as the Reynolds number is crucial for optimizing aerodynamic methods in early design phases.

Problem and Approach

At the Institute of Aerospace Systems at RWTH Aachen University a so-called "quasi-three-dimensional" (2.5D) approach was developed for the in-house "Multidisciplinary integrated conceptual aircraft design and optimization environment" (MICADO) [4] to predict laminar drag components on wing segments. Even though this process chain considers a possible influence of the Reynolds number via various assumptions, the question arises to which extent the desired degree of prediction accuracy is fulfilled. Therefore, this work is divided into the following two parts:

1. Investigation of the influence of the Reynolds number on various flow instabilities (section 3);
2. Derivation of steps to improve prediction accuracy of existing 2.5D approach (section 4).

Whereas the first part mainly focuses on basic studies using the 2.5D approach, the second part outlines the benefits of the adapted approach in the overall conceptual aircraft design. The latter is done by comparing the current and the adapted method in an application example using the entire MICADO process chain. The necessary basics for both parts will be presented in the next section.

2. Fundamentals

The well-known Reynolds number (Re) is defined as the ratio of inertia forces to friction forces within a fluid:

$$Re = \frac{\text{inertia forces}}{\text{friction forces}} = \frac{\rho_\infty \cdot u_\infty \cdot c}{\eta_\infty}. \tag{1}$$

Consequently, the Reynolds number of a wing flow is influenced by the air density (ρ_∞), the airspeed (u_∞), the

doi:10.25967/480188

chord length (c), and the dynamic viscosity (η_∞). Thus, the Reynolds number is usually varied during flight with every change in Mach number (Ma) and altitude (alt). In addition it is obviously varied along the wing span due to varying chord length. This will be taken into account in section 3. In aviation, the inertia forces are much larger than the friction forces [5]. However, the influence of the latter is noticeable in the boundary layer of a flow and cannot be neglected. For a flat plate, for example, a critical Reynolds number is defined in order to mark a threshold for the transition from a favorable laminar flow to a turbulent flow [6]. For the three-dimensional case, the boundary layer is not only influenced by 2D instabilities, but also by 3D instabilities. Both can cause premature transition and have therefore to be considered.

2.1. Instability mechanisms

On a backward-swept wing, velocity profiles occur not only in direction of flow, but also perpendicular to it. With regard to laminar flow, these velocity profiles induce the following three critical instability mechanisms:

- Tollmien-Schlichting instability (TSI)
- cross-flow instability (CFI)
- attachment-line transition (ALT)

Since the two-dimensional Tollmien-Schlichting (TS) waves are destabilized by a positive pressure gradient, they usually occur behind the maximum airfoil thickness. Thus, one established technique to suppress TSI is the favorable design of the airfoil; this technique is called "natural laminar flow" (NLF). In addition, these instabilities are predominant with respect to transition for wings with a leading-edge sweep of $\varphi_{\mathrm{LE}} \leq 10°$ [2], [7]. In contrast, three-dimensional cross-flow (CF) waves are amplified in regions with a strong negative pressure gradient. This is especially the case for regions behind the leading-edge of higher swept wings [8]. A promising technique to suppress CFI is to apply suction which decreases the flow velocity and thus stabilizes the flow. This technique is an example for "laminar flow control" (LFC). However, as a result of the contrary amplification behavior, simultaneous control of both TSI and CFI is only possible by combining the techniques described above. This combination of suction behind the wing leading-edge and airfoil shaping in the mid-chord region is called "hybrid laminar flow control". The last instability mechanism (ALT) can cause premature transition already at the attachment line, but it will not be considered within this study. For further information, the reader is referred to Reed [9].

2.2. Quasi-three-dimensional approach

To be able to investigate both TSI and CFI, a "quasi-three-dimensional" approach was developed. This approach couples the 2D flow solver MSES [10] with the stability analysis program suite STABTOOL [11], [12] in order to determine drag coefficients and the transition position via an iterative process using geometric and fluid-mechanical transformation methods. These transformation methods mainly use characteristic sweep angles of the wing as input data. Since the transition position is of special interest for the studies in section 3, a short, but not exhaustive overview of the underlying method is given. Detailed information can be found in Risse [13].

As a starting point, MSES calculates the 2D flow around an airfoil using a preset transition location as input. This results in a pressure distribution as well as lift- and drag coefficients. The 2D pressure distribution is then transformed to 3D using Lock's method [14]. Next, the resulting 3D pressure distribution is further prepared for internal usage by the STABTOOL program suite. After an analysis of the boundary layer, a linear stability analysis is performed using the e^N-method to calculate amplification rates of instability waves and the resulting envelopes of all curves, respectively. At every chordwise station these are integrated to so-called N-factors for both TS- and CF-waves, i.e. N_{TS} and N_{CF} values are calculated. The transition point is finally calculated using the so-called 2N-factor strategy. This approach is illustrated in Fig. 1.

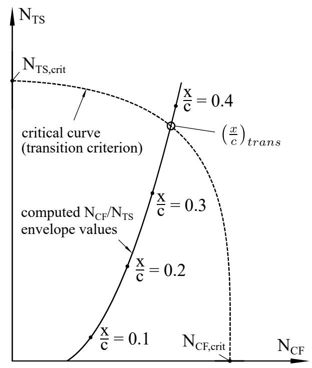

Fig. 1: Transition prediction using 2N-factor approach [13]

In principle, the transition point is assumed at the point where a computed curve of pairs of N_{TS} and N_{CF} intersects with a critical curve obtained from experiments. Whenever no intersection is found, the transition position is set to the point of laminar separation. At the end of each iteration, the transition point is fed back into the flow solver MSES as an updated input variable. The final, converged outputs of a single execution of this method are viscous as well as wave drag coefficients of a 2D airfoil with respect to the transition point. For further information, the reader is referred to Arnal [15] and Schrauf [12].

Since the calculation of drag polars requires numerous variations of both Mach number and lift coefficient, a huge number of evaluation steps within the preliminary aircraft design process is inevitable. To reduce calculation time, the process chain is extended by a database which mainly contains tables with laminar and turbulent aerodynamic data as a function of Mach number and lift coefficient. Initializing this database starts by selecting one key point for each given airfoil geometry along the span. More precisely, these geometric key points are the inner and outer stations of every given wing section. Then, for each geometric station, a predefined amount of Mach number and lift coefficient combinations is calculated with the 2.5D approach. The resulting data sets are written into a database. This database can be accessed within the aerodynamic MICADO module by querying it for various relative span lengths. For each query, the local viscous and wave drag coefficients are returned from the database. If a requested section lies between two geometric stations, the data is interpolated. The drag is then weighted by the belonging section areas. For a detailed description of the process chain, its various modules, and the further processing of the local drag coefficients, the reader is referred to Risse [13]. Nonetheless, as mentioned in section 1, the influence of the Reynolds number is so far only considered by the following assumptions:

- A variation of the flight altitude is not considered separately, since the drag does not undergo any significant changes at a constant transition position.
- A variation of the chord length is considered by means of a correction model using the theory of a flat plate.

The first assumption implies that there are always the same drag polars used in the aerodynamic calculation, regardless of the actual flight altitude. The second assumption is taken into account by calculating the partially laminar friction drag for each database query within the aerodynamic MICADO module. The underlying equations are for a full laminar flow $C_{d,fr,lam} = 1.328 \cdot Re_c^{-0.5}$ and for a full turbulent flow $C_{d,fr,turb} = 0.074 \cdot Re_c^{-0.2}$, respectively [8], [16]. These, in turn, are used to correct the viscous drag coefficients stored in the database via the following equation:

$$C_{d,vis,corr} = C_{d,vis,DB} \cdot \frac{C_{d,fr}\left(Re_{c,local},(x/c)_{tr,DB}\right)}{C_{d,fr}\left(Re_{c,DB},(x/c)_{tr,DB}\right)} \tag{2}$$

Consequently, the viscous drag coefficient $C_{d,vis,DB}$ stored in the database is corrected to the local chord length. However, it becomes clear that the same transition location is assumed in each case. In order to check whether these assumptions potentially lead to inaccurate predictions of laminar drag components, basic studies regarding the Reynolds number are conducted in the next section.

3. Influence of the Reynolds number on the transition position

The main objective of the following studies is to analyze the influence of the Reynolds number on the two major instability mechanisms (TSI and CFI) and on the transition position. To avoid mixing influences, a simplified reference wing is selected (see Fig. 2).

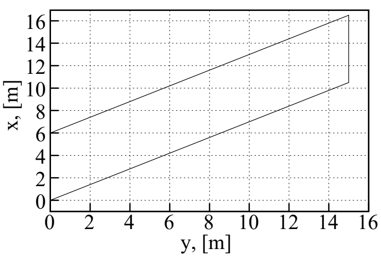

Fig. 2: Geometry of reference wing

As illustrated in Fig. 2, the reference wing is an untapered, swept wing with a half span of $b = 15\,\text{m}$ and a mean aerodynamic chord of $MAC = 6\,\text{m}$. By applying a sweep of $\varphi = 35°$, not only TSI, but also CFI will be considered without corrupting influences caused by a taper ratio. With regard to laminar flow, a typical HLFC airfoil with a maximum thickness of $(t/c) = 0.101$ is chosen (see upper part of Fig. 3).

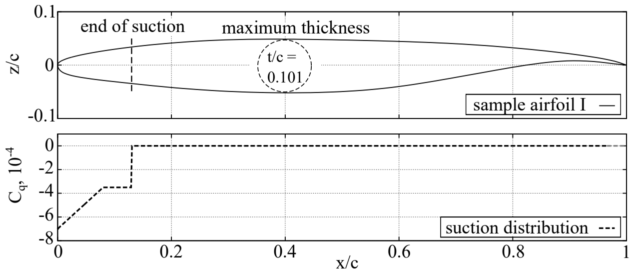

Fig. 3: Geometry of airfoil with chosen suction distribution

In addition, a constant suction distribution is selected along the wing span (see lower part of Fig. 3); this distribution is essentially based on a distribution used, for example, by Boeing for research purposes [17].

Since the Mach number, as the only one of the three input parameters mentioned in section 2, has a significant influence on the 3D pressure distribution, it will not be varied. This is the only way to ensure that the observed effects on the transition line can be traced back to the Reynolds number. Instead, it is set to $Ma = 0.85$ to take transonic effects into account. Also, the lift coefficient and altitude are set to $C_l = 0.6$ and FL 350, respectively.

3.1. Influence of the Reynolds number itself

Starting with the Reynolds number itself, this parameter is altered manually in the 2.5D approach while keeping all other parameters constant. Internally, this implies a variation of the flow density and with this of the kinematic viscosity. The variation interval covers Reynolds numbers from $Re = 2 \cdot 10^6$ to $Re = 1 \cdot 10^8$ (step size: $2 \cdot 10^6$); this is a typical range for Reynolds numbers in civil aviation [18]. In Fig. 4 several selected N-factor envelopes show the effect of an increasing Reynolds number on both TS- and CF-amplification rates.

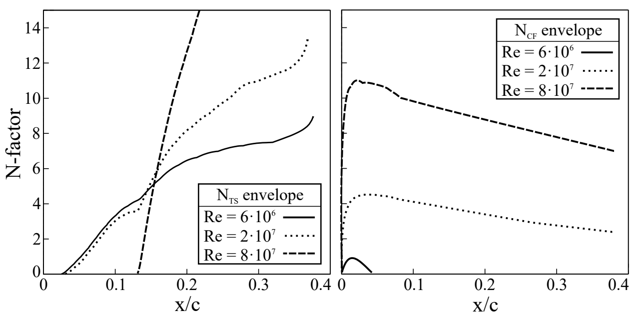

Fig. 4: N-factor envelopes for increasing Reynolds numbers

As can be seen in Fig. 4, the local gradients of the envelopes rise with increasing Reynolds numbers. This is due to a stronger amplification (and thus destabilization) of the respective instability waves and leads to higher N-factors.

The constant destabilization of both TS- and CF-waves results ultimately in the transition line and corresponding viscous drag coefficients plotted as functions of the Reynolds number in Fig. 5.

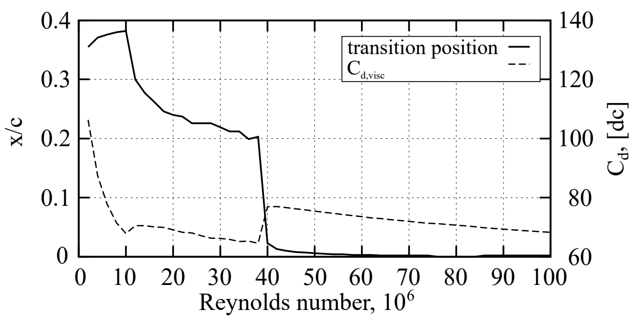

Fig. 5: Behavior transition position and viscous drag coefficient with increasing Reynolds number

Interestingly, two jumps of different strength can be observed in the transition line. For the lower Reynolds numbers, no intersection of N-factor pairs with the critical curve is found (and thus laminar separation is set as transition point). At $\mathrm{Re} \approx 1.0 \cdot 10^7$ a first jump occurs due to progressively growing TS-waves. With increasing Reynolds number, the transition location moves forward which is not only due to growing TS-waves, but also due to growing CF-waves. In between the different abrupt shifts of the transition line, the corresponding viscous drag coefficients decrease with increasing Reynolds number which is in good agreement with the theory of a flat plate [8]. At $\mathrm{Re} \approx 3.9 \cdot 10^7$ a second, more critical jump of the transition occurs. Since this abrupt shift results in a significantly increased viscous drag coefficient, Fig. 6 is used for a detailed analysis.

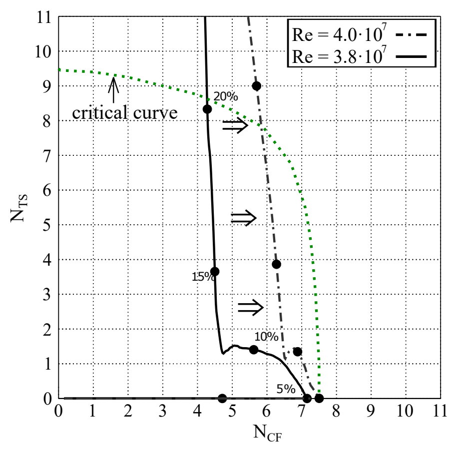

Fig. 6: Correlated N-factor curves for Reynolds numbers around the critical transition jump

Here, two correlated N-factor curves for Reynolds numbers around the critical transition jump (TrJp) from Fig. 5 are shown. The bold dots represent N-factor pairs at their corresponding relative chord lengths. Recalling section 2, the transition position is defined as the point where the correlated curve intersects with a curve derived from experiments; in this work, critical N-factor values of $N_{TS,crit} = 9.5$ and $N_{CF,crit} = 7.5$ are used. It can be observed that an increasing Reynolds number leads to a shift of the correlated curve to the right side. Since the abscissa represents the N_{CF}-factors, this shift is mainly due to growing CF-waves as illustrated in the right part of Fig. 4. For $\mathrm{Re} = 3.8 \cdot 10^7$, the correlated curve narrowly misses an intersection at the right edge and starts to rise due to growing TS-waves for increasing relative chord length. This eventually leads to an intersection (and thus transition) at around $(x/c) \approx 0.2$. For $\mathrm{Re} = 4.0 \cdot 10^7$, however, the correlated curve is shifted so far to the right that the critical curve is immediately exceeded at the right corner. This results in the observed, critical jump of the transition to the leading-edge of the wing.

To conclude, varying the Reynolds number itself leads to a progressive amplification of both TS- and CF-waves. This results in abrupt jumps of the transition position which can influence the viscous drag coefficient of a flow significantly.

3.2. Influence of altitude and chord length

Next, the influence of the flight altitude and the chord length is analyzed by varying these parameters both individually and simultaneously. The altitude is varied from FL 250 to FL 400 with a step size of 1000 ft; the chord length from the wing in Fig. 2 is varied from 2 m to 14 m with a step size of 0.5 m.

The amplification rates of the instability mechanisms show the same behavior as in section 3.1, i.e. the respective instability waves are progressively growing with increasing Reynolds number. More intriguing are the resulting transition curves, which are presented in Fig. 7.

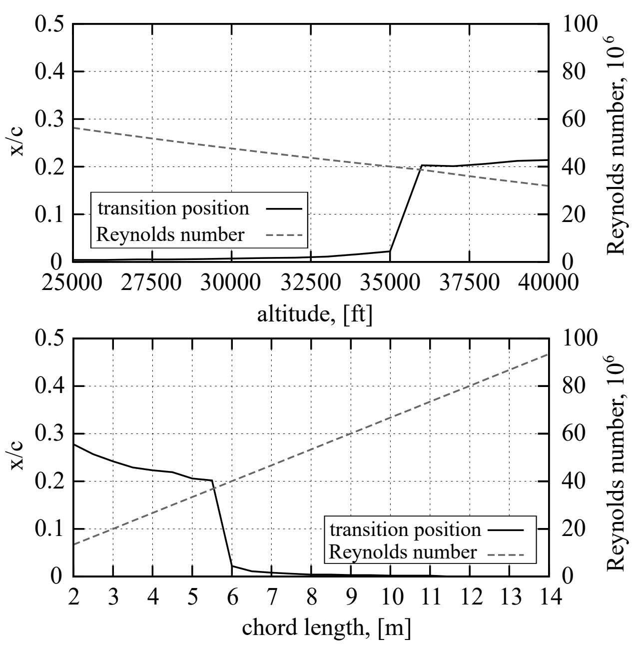

Fig. 7: Influence of different Reynolds number parameters on the transition position

Here, the relative transition position and the Reynolds number are plotted as a function of the flight altitude (upper part) and as a function of the chord length (lower part), respectively. As can be clearly seen, both plots also contain critical shifts of the transition position if the parameter is varied individually. In addition, these shifts occur roughly at the same Reynolds numbers. To narrow this possible threshold down, both parameters (altitude and chord length) are varied simultaneously. For detailed analysis, the variation step size is set to $\Delta_{\text{alt}} = 1000\,\text{ft}$ and $\Delta_{\text{c}} = 0.05\,\text{m}$. The focus is on the Reynolds number range around the abrupt shift to the wing leading-edge classified as critical in the previous studies ($3.8 \cdot 10^7 \leq \text{Re} \leq 4.2 \cdot 10^7$). The results are listed in Tab. 1; the parameter Re_{TrJp} represents the threshold from which the transition jumps to the leading-edge.

Tab. 1: Results of simultaneously varied Reynolds number parameters

FL	chord length [m]	Re_{TrJp}
250	4.25	$3.988 \cdot 10^7$
260	4.40	$3.996 \cdot 10^7$
270	4.55	$3.997 \cdot 10^7$
280	4.70	$3.994 \cdot 10^7$
290	4.85	$3.985 \cdot 10^7$
300	5.00	$3.971 \cdot 10^7$
310	5.20	$3.991 \cdot 10^7$
320	5.35	$3.967 \cdot 10^7$
330	5.55	$3.975 \cdot 10^7$
340	5.75	$3.976 \cdot 10^7$
350	5.95	$3.972 \cdot 10^7$
360	6.15	$3.962 \cdot 10^7$
370	6.45	$3.964 \cdot 10^7$
380	6.75	$3.954 \cdot 10^7$
390	7.15	$3.964 \cdot 10^7$
400	7.50	$3.991 \cdot 10^7$

In Tab. 1 the values of the third column (Re_{TrJp}) oscillate slightly; however, these deviations are not significant and can be traced back to numerical inaccuracies within the MSES-STABTOOL process chain. Therefore it becomes clear that even with simultaneous variation of the flight altitude and the chord length a constant parameter Re_{TrJp} can be observed.

In summary, the choice of the varied Reynolds number parameter is irrelevant, since any transition jump—under otherwise constant environmental conditions—can be attributed to exceeding a critical limit of the Reynolds number. Consequently, a critical Reynolds number $\text{Re}_{\text{crit,TrJp}}$ is defined for the further course of this work. This parameter is generally based on the known critical Reynolds number of the laminar-turbulent transition on a flat plate; in this context, however, exceeding $\text{Re}_{\text{crit,TrJp}}$ causes a critical transition jump on a 3D wing.

3.3. Influence of geometrical parameters on the critical Reynolds number

During the iterative aircraft design and optimization, various wing geometries are examined before the final geometry is determined. As a major constraint, the STABTOOL input data has been kept constant in the previous studies. This was done by using a reference wing without different geometrical sections, i.e. no different sweep angles and airfoils in spanwise direction. Furthermore, the Mach number and the lift coefficient have been kept constant. Nonetheless, for state-of-the-art wing geometries of commercial aircraft, these assumptions are not realistic. For example, a kinked wing comes with different sweep angles along the span. Obviously, due to the geometric and fluid-mechanical transformation methods, the pressure distribution and thus the STABTOOL input data are strongly dependent on geometric parameters. Therefore, when analyzing a more realistic wing geometry, different $\text{Re}_{\text{crit,TrJp}}$ must inevitably be expected. To briefly illustrate this, another airfoil geometry, which mainly differs in the radius of the leading-edge, is examined. In order to solely consider the influence on $\text{Re}_{\text{crit,TrJp}}$, but at the same time to enable a consistent comparison with the previous results, the reference wing presented at the beginning of section 3 is used as a starting point. Similar to the previous approach, the 2.5D method is used for analysis, whereby the local chord length is selected as the parameter for varying the Reynolds number; this is due to the proportional correlation (cf. Eq. (1)). The new sample airfoil (II) as well as the resulting transition curve are presented in the upper and lower part of Fig. 8.

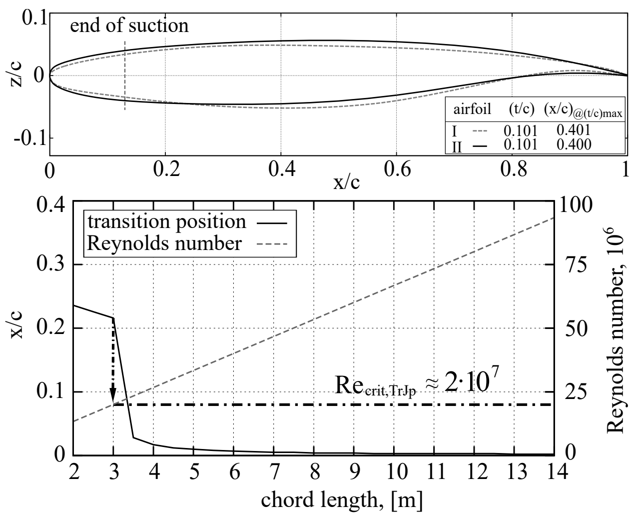

Fig. 8: Influence of different airfoil on transition jumps

Fig. 8 shows that airfoil (II) leads to a completely different threshold value for the critical transition shift. In numbers, the previous threshold of $\text{Re}_{\text{crit,TrJp}} \approx 4.0 \cdot 10^7$ is reduced by about 50 %. This confirms the assumption from above, i.e. different threshold values $\text{Re}_{\text{crit,TrJp}}$ must be expected for a wing with several geometrically different sections.

To summarize, the assumption of a constant transition location in Eq. (2) eventually leads to significant inaccuracies in the prediction of laminar drag components. This is because the current database method does not explicitly consider the geometrically characteristic threshold values $\text{Re}_{\text{crit,TrJp}}$. Thus, in the next section, it will be examined whether the effects of exceeding such a threshold are greater than those taken into account by the assumptions and substitute models within the current 2.5D approach.

4. Adapted database method and comparative application

To address possible weak points of the current database method, an adapted method will be discussed next. In an application example both the current and the adapted methods will then be compared with each other.

4.1. Adapted database method

The initial idea of using a database will not be changed, as this approach brings several advantages in conceptual aircraft design, e.g. reduced calculation time and the possibility to manually adjust numerical uncertainties. Instead, the current method will be adapted in order to increase prediction accuracy by taking aerodynamic effects more precisely into account. To avoid increasing the dimensions of the database, it is assumed that the wing geometry is given. The adaption involves a total of 4 process steps which are presented in Fig. 9.

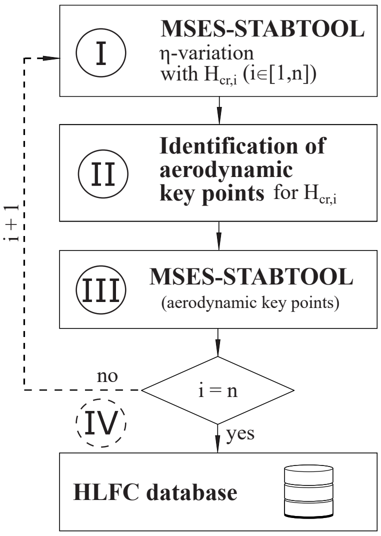

Fig. 9: Process overview of adapted database method

In the first step, the known wing geometry is analyzed with the MSES-STABTOOL process chain. This is done for the initial flight altitude and the design point (Ma_{des}, $C_{l,des}$). The latter is chosen on the assumption that the aircraft is usually operated at the design point. A variation step size of $\eta = 0.05$ is selected in order to make a first rough estimate of the transition and drag curve across the wing. If geometric parameters change along the span, these relative span positions are also included in the variation interval. This ensures that any influence (geometric and aerodynamic) is mapped. The final choice of aerodynamic key points (step II) will be discussed in detail in section 4.2.

In the third process step, the predefined amount of Mach number and lift coefficient combinations (see section 2.2) is calculated for every final aerodynamic key point.

To further increase prediction accuracy, the whole process chain can be repeated for varying cruise altitudes in an optional fourth step. Finally, all calculated data sets are written into the database.

4.2. Preparation of comparative analysis

The overall objective of the following study is to demonstrate the benefit of the adapted database method. For this purpose a reference aircraft was designed in MICADO which is based on an Airbus A350-900. The 3D view and the kinked wing geometry are illustrated in Fig. 10; the respective wing parameters are listed in the box in the left corner.

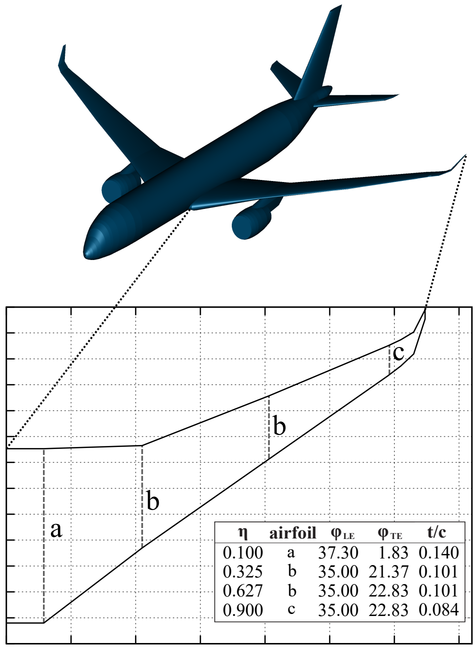

Fig. 10: 3D view and wing geometry of reference aircraft from MICADO

Additionally, the parameters of the design mission as well as the associated mass components are listed in Tab. 2.

Tab. 2: Design parameters of reference aircraft

Parameter	Unit	Value
Design range	NM	8100
Altitude$_{cr}$	ft	35000
Ma$_{cr}$	-	0.85
PAX	-	325
Operating empty mass (OEM)	t	147.8
Payload	t	30.9
Blockfuel (BF)	t	94.1
Maximum take-off mass (MTOM)	t	280.8

As usual, the range is reduced for the study mission; all following studies use a mission with a range of 4000 NM. Before comparing the two methods, the database has to be created. The preparatory steps, which include in particular the selection of key points, are described below for both methods.

In section 2.2 it was already mentioned that the current database method requires a geometric key point to be selected for each airfoil. The data in Fig. 10 indicates that there are two key point candidates for airfoil "b" for the middle wing section ($\eta_{cand,1} = 0.325$ and $\eta_{cand,2} = 0.627$); this is because the inner and outer stations of this section contain the same airfoil. Since the current method intends to only create one data set for each airfoil, the geometry station is used at which a larger change in the sweep occurs with respect to the prior section. Thus, three geometric key points at the relative span positions $\eta_1 = 0.1$, $\eta_2 = 0.325$ and $\eta_3 = 0.9$ are selected. However, no realistic lift-to-drag ratios are predicted for the first geometric key point. This is due to the fact that the influence of CF-waves, as they increasingly occur in the root area, is not yet correctly mapped within the 2.5D approach [19]. The false prediction of too high drag coefficients in the root area is in the following avoided by using an alternative procedure from Risse [13]. This approach uses a simplified reference wing to calculate the root airfoil at its relative span position; the resulting data set as well as the data sets from the other geometric key points $\eta_2 = 0.325$ and $\eta_3 = 0.9$ are also added to the database.

The adapted method follows the process steps from Fig. 9. The resulting drag coefficient curves from the first step are presented in Fig. 11.

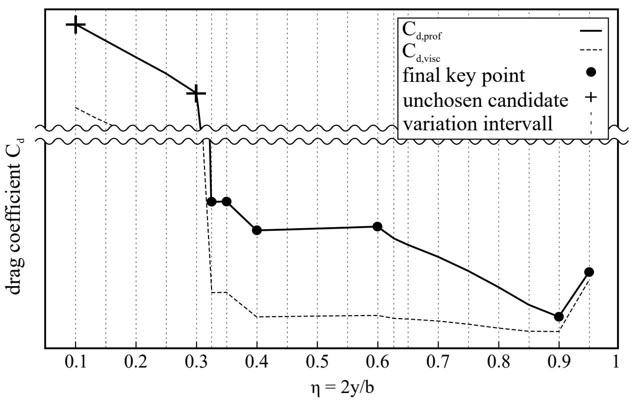

Fig. 11: Results from process steps I and II

The second process step is to analyze the profile drag $C_{d,prof}$ $(= C_{d,visc} + C_{d,wav})$ coefficient curve for significant changes in order to define aerodynamic key points (dots in Fig. 11). This is advantageous, since on the one hand non-critical transition jumps are not further considered and on the other hand the effects of a changing geometry are taken into account. It can be observed that eventually not all key point candidates (crosses in Fig. 11) will be chosen as final aerodynamic key points. This is again due to the over-prediction of the influence of CF-waves. Here, the data set for the simplified reference wing will also be used for the root section. This leads in total to 7 aerodynamic key points (including the root station from the simplified reference wing).

To demonstrate the effect of the different database methods, the converged reference aircraft is analyzed without further MICADO iterations. Thus, the pure influence of different aerodynamic data sets can be investigated without a possible snowball effect of the MTOM. The focus is on the elaboration of the aerodynamic differences with a final statement regarding the effect on the necessary blockfuel. The results are presented in the next section.

4.3. Results of comparative analysis

In Fig. 12 the laminar areas for $(L/D)_{opt}$ are shown for both the current and the adapted database method.

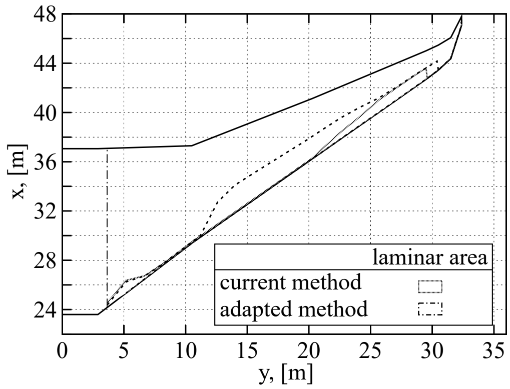

Fig. 12: Wing geometry with laminar areas

Since the calculation up to the kink is based on an interpolation with a data set determined on the simplified reference wing, the transition and drag curve in this section are identical for both methods. Furthermore, the flow is assumed to be fully turbulent after the last key point, because of highly amplified 3D flows at the wing tip. However, there are significant differences between these sections:

For the current method the flow is predicted to be turbulent over the entire chord length up to $\eta = 0.627$. This is due to the fully turbulent flow at the geometric key point at $\eta = 0.325$, and the fact that only one data set is stored in the database for airfoil "b". Thus, for this section it is always the same data set used. The laminar area then grows linearly to the last geometric key point, since the data sets for the two airfoils "b" and "c" are interpolated.

In contrast, the adapted method predicts a transition jump which leads to a significantly larger laminar area; this is mainly due to the additional aerodynamic key points around the kink region. After weighting by the reference wing area, the total wing coefficients are given in Tab. 3. In order to better compare the aerodynamic accuracy of the two methods, the results are shown for a constant lift coefficient of $C_L = 0.4$.

Tab. 3: Result overview for $C_L = 0.4$ (FL 350)

Coefficient	DB method		Deviations	
	current	adapted	Δ [dc]	Δ [%]
C_L	0.4	0.4	-	-
$C_{D,visc}$	0.01090	0.01045	−4.5	−4.13
$C_{D,wav}$	0.00137	0.00135	−0.2	−1.46
$C_{D,ind}$	0.00674	0.00674	-	-
$C_{D,total}$	0.01901	0.01854	−4.7	−2.47

As expected, due to the constant lift coefficient, the induced drag shows no deviations. However, Tab. 3 shows that the application of the adapted method leads to a reduction of almost 5 drag counts (dc) or 2.47 % with respect to the total drag coefficient at a constant lift coefficient. This can be directly traced back to the larger laminar area and its influence on the friction drag. Since this data only mirrors one mission point, the predicted blockfuel demand for the whole study mission over 4000 NM is illustrated in Fig. 13.

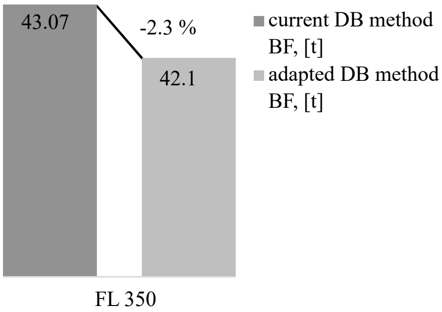

Fig. 13: Predicted BF demand for FL 350

Overall, using the adapted method leads to a reduction of the necessary BF by approx. 1000 kg or 2.3 %, respectively. Against the background that the HLFC technology is supposed to have a savings potential of 10 % – 20 % [2], this is a significant increase in prediction accuracy. Consequently, the potential of HLFC technology is depicted more precisely by taking aerodynamic key points into account.

The current DB method does not take any aerodynamic influences of an altitude variation in cruise flight into account. Thus, the aerodynamic calculation is performed once; these results are then used for mission analysis at varying altitudes. In contrast, the adapted database methodology optionally includes the consideration of different flight altitudes (see Fig. 9). Therefore the systematic comparison is not only carried out for FL 350, but also for two further altitudes (FL 300 and FL 400) in order to determine a possible inaccuracy of the current procedure.

Since the Reynolds number decreases with altitude, the spanwise position of the transition jump is shifted; this is because the critical threshold $Re_{crit,TrJp}$ is only exceeded with greater chord length. In short, this leads to the identification of different aerodynamic key points. For FL 300 and FL 400 there are in total 7 and 5 aerodynamic key points. Fig. 14 shows to what extent the BF demand varies when taking these aerodynamic key points and the data sets created for the respective altitude into account.

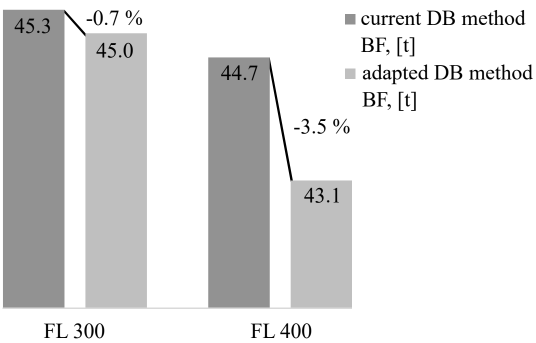

Fig. 14: Predicted BF demand for FL 300 and FL 400

It can be observed that the application of the adapted method (and thus the consideration of different altitudes) also leads to differences in the prediction of the necessary BF. On the one hand, for FL 400, an additional reduction of the BF demand of approx. 1500 kg or 3.5 % is achieved, as the laminar area for FL 400 is larger than for FL 350 due to the mentioned shift of the transition jump to a higher chord length. On the other hand, the results for FL 300 differ by only about 0.7 %, since the transition jump is shifted to a smaller chord length, and thus the laminar area approximates the prediction of the current method for FL 350.

It can therefore be noted that the procedure proposed in the process diagram in Fig. 9 covers more eventualities that may occur with an altitude variation, and the most accurate prediction can only be achieved if the optional altitude variation of the adapted DB method is considered.

Nonetheless, it must be stated that the more aerodynamic key points and altitudes have to be considered, the longer it takes to set up the database. In terms of required computation time on a standard desktop PC, the current method takes approx. 13.5 hours for initialization, whereas the adapted method takes about 31.5 hours (without optional altitude variation). If the fourth step of the adapted method is taken into account, the initialization time adds up to approx. 70 hours. Consequently, the main objective in preliminary aircraft design with integrated HLFC technology should be to completely avoid any abrupt transition shifts along the wing span. This would directly influence the required number of aerodynamic key points. Since the suction distribution is the most promising approach to achieve this, possible starting points will be briefly discussed below.

4.4. Influence of the suction distribution

The work initially focused on basic studies to investigate the influence of the Reynolds number in detail. For this reason, the suction distribution in Fig. 3 has been kept constant in the previous studies. However, the significant influence of a variation of the suction distribution's strength has already been shown [13]. For example, stronger suction at the leading-edge dampens cross-flow instabilities in particular and delays (and in best case prevents) the resulting transition jump. In combination with the findings of this work, this is equivalent to an increase of the critical threshold $Re_{crit,TrJp}$. Furthermore, a variation of the suction length leads to a shift of the transition line [13]. However, the transition jump or the limit value $Re_{crit,TrJp}$ is not affected by this.

Since the transition line already shows sensitivities when a single parameter such as the maximum suction strength is varied, it appears reasonable to examine not only individual parameters, but also completely different suction distributions in the preliminary aircraft design. In the MSES-STABTOOL process chain, parameters of the suction distribution can be varied; however, this is limited to individual linear intervals. Nonetheless, there are already mathematical models available in literature that use the Lagrange multiplier method to assign an optimum suction to each N-factor [20]. As a result, optimum suction is theoretically variable both along the wing span and across the chord length at any time of the flight mission. It is nevertheless questionable to what extent these models are applicable to reality or practicable in application, especially with regard to the necessary complexity of the suction system. For this reason, coupling of the N-factors and the suction system is dispensed with. In order to enable future studies for different suction distributions, the process chain is extended by an optional selection of different suction types. The implemented variation possibilities of suction distributions are exemplary illustrated in Fig. 15.

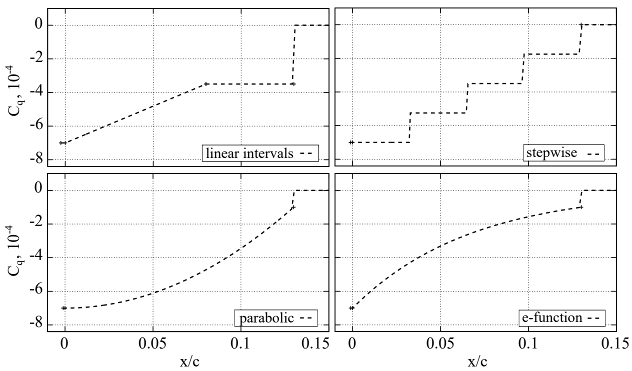

Fig. 15: Visualization of different suction distributions

As can be observed, the distributions follow typical mathematical equations. These can be varied in the same way as the linear interval suction using characteristic parameters. To illustrate the effects of the different suction types on the transition line, process step 1 is repeated for FL 350. The respective parameters are identical to those in Fig. 15; i.e. for a consistent comparison, the maximum suction strength is always the same. The results are presented in Fig. 16.

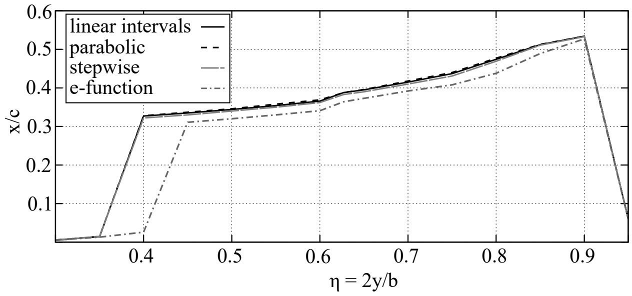

Fig. 16: Influence of different suction distributions on transition position

It becomes clear that for the exponential suction distribution the transition jump to the leading-edge already occurs at a lower Reynolds number. This is due to a weaker damping of the CF-waves. Consequently, exponential suction with selected parameters is unsuitable to avoid a transition jump. Contrary, step wise as well as parabolic suction lead to almost identical transition and drag curves compared to the reference. It follows that an identical aerodynamic result is also possible through different suction distributions. This leads to a starting point for future optimizations of HLFC technology. It appears reasonable to supply the relative span positions with an optimal suction distribution, i.e. with an optimal suction type and corresponding parameter settings from an overall perspective. This extension basically follows the logic of the above-mentioned mathematical model, although there is no constant variation of the suction with regard to the necessary complexity of the HLFC system. The coupling of the suction distribution with the relative span position has already been investigated by Pe [21]. As the spanwise position increases, suction is both weaker and shorter. This can be a starting point for future studies within MICADO.

5. Conclusion

In conceptual aircraft design, the usage of simplified methods to predict efficiency gains of new technologies is inevitable. Thus, it is crucial to understand the influence of a fundamental key variable such as the Reynolds number in order to optimize the 2.5D method for HLFC assessment implemented in the preliminary aircraft design environment MICADO. For this purpose, the influence of the Reynolds number (and its parameters) on the transition position and on various instability mechanisms was examined in detail. At constant freestream conditions, the amplification of the individual instabilities could be fundamentally attributed to the Reynolds number as a decisive factor. Based on the limit value of the laminar-turbulent transition for a flat plate, a critical threshold of the Reynolds number ($Re_{crit,TrJp}$) was therefore defined for the flow over a wing. The exceeding of this threshold leads to a jump in the transition. In addition, the influence of relevant geometry parameters of the wing on the previously defined critical threshold was briefly discussed. It became clear that these have a significant influence on the critical value and the transition jumps. Based on the collected findings, the necessity of adapting the aerodynamic process within MICADO was derived in order to adequately reflect the influence of the Reynolds number. This adapted method allows simultaneous consideration of both aerodynamic and geometric influences on laminar drag components. Focusing on the profile drag for initial identification of aerodynamic key points ensures that transition jumps are considered. The advantages of the adapted database methodology were demonstrated through various studies. Here, a significant improvement in the prediction accuracy of laminar drag components has been shown in comparison to the current database method. This is due to the consideration of additional aerodynamic key points for the initialization of the database. Furthermore, it was shown that a variation in altitude is not negligible due to its influence on the Reynolds number. Overall, the adapted method results in an improved accuracy of the aerodynamic analysis within MICADO. Finally, the possibilities for further development of the adapted database method were discussed. Although relevant transition jumps are taken into account by the adapted DB method, a complete avoidance of these abrupt shifts is desirable. Especially the variation of the suction parameters is a promising starting point. In this context, not only the variation of the suction strength, but also a variation of the basic form of the suction distribution were discussed. In future studies, the usefulness of coupling the suction distribution to the relative span position should be investigated. However, these studies should always question the physical feasibility with regard to system complexity, space requirements and the necessary power withdrawals of the HLFC system.

References

[1] Schrauf, G.: Status and perspectives of laminar flow. The Aeronautical Journal, Vol. 109, No. 1102, pp. 639–644, 2005.

[2] Joslin, R. D.: Overview of Laminar Flow Control: Tech. Rep. NASA/TP-1998-208705, 1998.

[3] Redeker, G.; Wichmann, G.: Laminarhaltung an ungepfeilten und gepfeilten Flügeln: Tech. Rep. AD 02 02 005, 1995.

[4] Risse, K.; Anton, E.; Lammering, T.; Franz, K.; Hoernschemeyer, R.: An Integrated Environment for Preliminary Aircraft Design and Optimization. In 53rd AIAA/ASME/ASCE/AHS/ASC Structures, Structural Dynamics and Materials Conference: SciTech 2012, American Institute of Aeronautics and Astronautics, 2012.

[5] Truckenbrodt, E.: Fluidmechanik: Band 1: Grundlagen und elementare Strömungsvorgänge dichtebeständiger Fluide, Berlin, Heidelberg: Springer, 2008.

[6] Schröder, W.: Fluidmechanik. In Aachener Beiträge zur Strömungsmechanik. Aachen: Mainz, 2004.

[7] Saric, W.; Reed, H. L.: Toward Practical Laminar Flow Control: Remaining Challenges. In 2nd AIAA Flow Control Conference, AIAA, 2004.

[8] Schlichting, H.; Gersten, K.: Grenzschicht-Theorie, Berlin, Heidelberg: Springer, 2006.

[9] Reed, H. L.; Saric, W. S.: Stability of Three-Dimensional boundary layers. Annual Review of Fluid Mechanics, No. 21, pp. 235–284, 1989.

[10] Drela, M.: A User's Guide to MSES 3.05: User Manual, 2007.

[11] Schrauf, G.: COCO: A Program to Compute Velocity and Temperature Profiles for Local and Nonlocal Stability Analysis of Compressible, Conical Boundary Layers with Suction: Tech. Rep. ZARM, 1998.

[12] Schrauf, G.: LILO 2.1: User's Guide and Tutorial: GSSC Tech. Rep. 6, 2006.

[13] Risse, K.: Preliminary Overall Aircraft Design with Hybrid Laminar Flow Control: Vorentwurf von Flugzeugen mit hybrider laminarer Strömungskontrolle. RWTH Aachen University, PhD thesis, 2016.

[14] Lock, R. C.: An Equivalence Law Relating Three- and Two-Dimensional Pressure Distributions: Reports and Memoranda, 3346, 1964.

[15] Arnal, D.; Casalis, G.; Houdeville, R.: Practical Transition Prediction Methods: Subsonic and Transonic Flows. In Advances in Laminar-Turbulent Transition Modelling. Rhode St. Genesé, Belgium, pp. 7-1–7-34, 2008.

[16] Schlichting, H.; Truckenbrodt, E.: Aerodynamik des Flugzeugs - Erster Band: Grundlagen aus der Strömungsmechanik. Aerodynamik des Tragflügels (Teil I), Berlin, Heidelberg: Springer, 2001.

[17] Hood, R. V.; Middleton, D. B.; Hanks, G. W.; Moyer, A. E.; Ledbetter, G. E.; Nagel, A.L., et al.: Hybrid Laminar Flow Control Study: Final Technical Report: Contractor Report, NASA/CR-165930, 1982.

[18] Lissaman, P.: Low-Reynolds-Number Airfoils. Annual Review of Fluid Mechanics, No. 15, pp. 223–239, 1983.

[19] Schueltke, F.; Stumpf, E.: Cross-flow effects regarding laminar flow control within conceptual aircraft design. Aircraft Engineering and Aerospace Technology: An International Journal (AEAT), Vol. 89, No. 4, pp. 620–631, 2017.

[20] Balakumar, P.; Hall, P.: Optimum Suction Distribution for Transition Control. Theoretical and Computational Fluid Dynamics, Vol. 13, No. 1, pp. 1–19, 1999.

[21] Pe, T.: HLFC Technology Integration and Assessment: Tech. Rep. FST-PB-2013-32, 2013.